International Research Institute of Stavanger

www.iris.no

Anders Nermoen[1,2], Espen Jettestuen[2,3]

[1] IRIS AS
[2]University of Stavanger
[3]University of Oslo

Quantitative Image Analysis

Phase II

Report IRIS - 2016/

Project number:	7001127
Project title:	Quantitative SEM micrograph image analysis
Client(s):	The National IOR Centre of Norway
Distribution restriction:	According to the NIOR centre policy

Stavanger, 22.09.2016

Anders Nermoen	Sign.date
Project Manager	

Olav Aursjø	Sign.date
Project Quality Assurance	

Ying Guo	Sign.date
Director Enhanced Oil Recovery	

Stavanger, 22. September 2016

Anders Nermoen, Project Manager

Contents

Summary

In the chalk reservoirs at the Norwegian Continental Shelf (NCS) significant injectivity loss when seawater is injected, has been reported. In fractured reservoirs, in the presence of oil and water, several factors could be at play to explain the permeability loss as e.g. relative permeability and matrix-fracture flow effects (i.e. lost injectivity). However, experiments of unfractured Liège chalks in one-phase matrix flow have also revealed large permeability losses during chemo-mechanical compaction. Detailed geochemical analysis of chalk cores exposed to continuous flow of strong $MgCl_2$ brine has revealed that chemical reactions and mineral dissolution and precipitation do take place. However, the observed permeability loss has not been satisfactory explained via changes in porosity and Brunauer-Emmett-Teller (BET) theory for specific surface area measurements from the adsorption of gas molecules. Given that, other mechanisms are required to describe the rest of the observed decline. We propose that micro-structural changes from dissolution/precipitation effects lead to increased hydraulic friction. However, until now we the required tools were missing to study changes in objective and quantitative ways.

Searching for microstructural changes, a new image analysis software has been developed (in Python). The aim of the project has been to develop a rapid and numerically stable segmentation algorithm that can be used to find grain boundaries of SEM images and to analyze statistically how the grains (i.e. domains) change before and after flow-through experiments. A fast implementation scheme is developed based on minimizing the Mumford-Shah functional [Mumford & Shah (1989), Strekalovskiy & Cremers (?), Weinmann et al (2014)]. This functional has been used in signal and image processing for edge detection, de-noising and segmentation. The extension proposed here is using a N-dimensional spin model, similarly to Brox & Cremers in 2009. In the presented 'fast implementation' scheme each pixel is changed between the different spin-states and a penalty energy function is calculated from the surface energy calculated from neighboring pixels (if they belong to another domain) and a grey-scale match with the original image. The segmented images is meant to match mineral grains of SEM-images.

The overall goal is to provide objective and quantifiable measures for the microstructural changes. With such measures more detailed hypotheses can be tested to better understand why permeability is reduced, by incorporating not only porosity and specific surface area, but also changes to the microscopic granular morphology. The precise value of each parameter that is the outcome of the implementation can be debated. However, assuming that the error made is systematic, the software can be used to quantify the relative changes before and after flooding. In this report we i) describe the rationale behind the strive for microstructure objective measures, ii) run analysis tool on a specific case consisted of an unflooded end-piece, and slice 1 and 6 of the Liegè chalk core flooded for 516 days. Changes to the grain size distribution is observed where the number of small grains are increased in slice 1. Increasing the number of small grains reduce the pore throat distribution and hence increase the hydraulic flow resistance through the core. A striking match with the BET specific surface area was obtained. This is promising to the application and future developments of this method. In the end, a detailed technical report authored by Espen Jettestuen of the implementation scheme is provided.

1 Introduction

A fast implementation scheme has been employed to quantify the morphological changes observed before flooding (see *Figure 1*) and slice 1 and 6 after 516 days of $MgCl_2$ flood (see *Figure 2*). A description of the chemical alteration of this exact experiment has been reported in [Zimmermann et al. (2014)], and SEM-EDS and the BET analyses were reported by Hildebrand-Habel in JCR7 meetings [T. Hildebrand-Habel JCR-7 (2012)]. The resulting dynamics acquired during the core test and the changes before and after test is described in *Figure 3*. The experiments has been conducted by Reidar I. Korsnes within the "Water weakening of chalk – at insitu reservoir conditions", a KMB Petromaks II project that were led by Merete V. Madland and Aksel Hiorth [Water weakening of chalk – Petromaks II project (2014)]. As has been reported in the reports above, the chalk core has undergone significant chemical alteration. The consequences of the microstructure can be seen comparing SEM images in *Figure 1* and *Figure 2* where the unflooded and slice 1 (near inlet) and 6 (near outlet) are seen. As shown in [Zimmermann *et* al (2012)], and also documented in the EDS-results reported here (see Table 1, 2 and 3), complete alteration from calcium carbonate to magnesite is recorded the first slice, and ¾ into the second slice where a sharp front, between calcium carbonate domination and magnesite domination is observed (see *Figure 3*d). At the same time, the specific surface area measured using the BET technique has been shown to double throughout the core from the inlet to the outlet, even though calcite-magnesite transition was focused to the first 2 slices. This fact is peculiar, as it seems like the change in specific surface area is not only given by the degree of chemical reworking and that other factors play a role in the doubling in specific surface area. Remark however, that the Mg-content increased from approx. 0.2% originally (see Table 1)) to more than 2% for from slice 3-6 and to more than 20% in slice 1 and 2. As such, chemical reactions took place throughout the core, although to a less extent downstream, but sufficient for the specific surface area to double.

As shown in *Figure 3*a the hydraulic permeability was reduced drastically during the first 180 days of flooding. By using the same analysis as was developed in [8],

$$k = \frac{\phi^3}{S^2 \tau K} \rightarrow \left(\frac{k}{k_0}\right)\left(\frac{\phi_0}{\phi}\right)^3 = \frac{\tau_0 K_0}{\tau K}\left(\frac{S_0}{S}\right)^2 \quad (1)$$

we find that by using the Carman-Kozeny approach the observed permeability was reduced more than what could be explained by the observed changes to porosity and specific surface area. A doubling in the specific surface area lead to a factor 4 decline in the permeability. The porosity development is calculated from the volumetric change and a simplified chemical alteration rate as reported in (Nermoen *et* al. 2016), since the exact numbers in this specific case could not be found in the database. In *Figure 3*b the observed permeability loss is scaled with the estimated porosity evolution (to the power 3). Consequently, the right hand side of Eq. (1) (i.e. the rescaled changes in Kozeny constant, Tortuosity, and specific surface area) approach 10. The doubling in specific surface area can account for a factor 4 out of the observed change.

As such, to understand the observed permeability loss it is inadequate to include the porosity loss and specific surface area doubling, as this effect combined can only describe 40% of the observed variance. We therefore conclude that other mechanisms are at play possibly related to microscopic morphological changes being important to the

observed permeability dynamics. However, until now, these morphological changes has only been reported using subjective and descriptive tools. This is not good enough to obtain firm understanding of what is going on. As such, given the observed porosity and specific surface area changes the question remains: which mechanisms are at play in the large hydraulic permeability reduction during chemo-mechanical compaction of chalk? In order to address this issue, there is a need to develop new objective and quantitative tools to measure the microscopic morphological changes. This report describes an attempt to develop such tools. The idea is that with this tool we are a little closer to understand permeability changes across the cores during compaction and chemical flow.

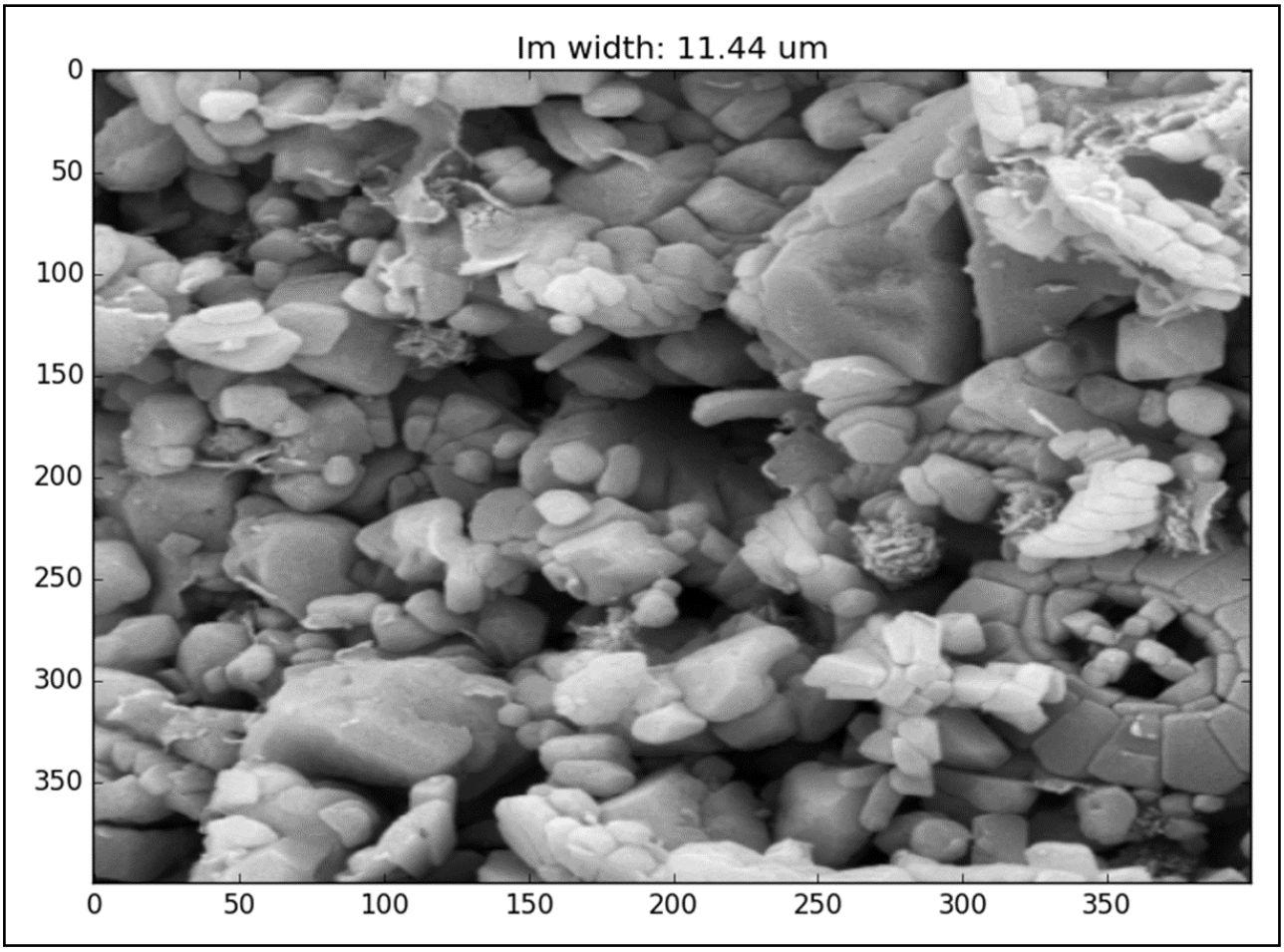

Figure 1 SEM image of unflooded Liegè chalk from the untested inlet slice.

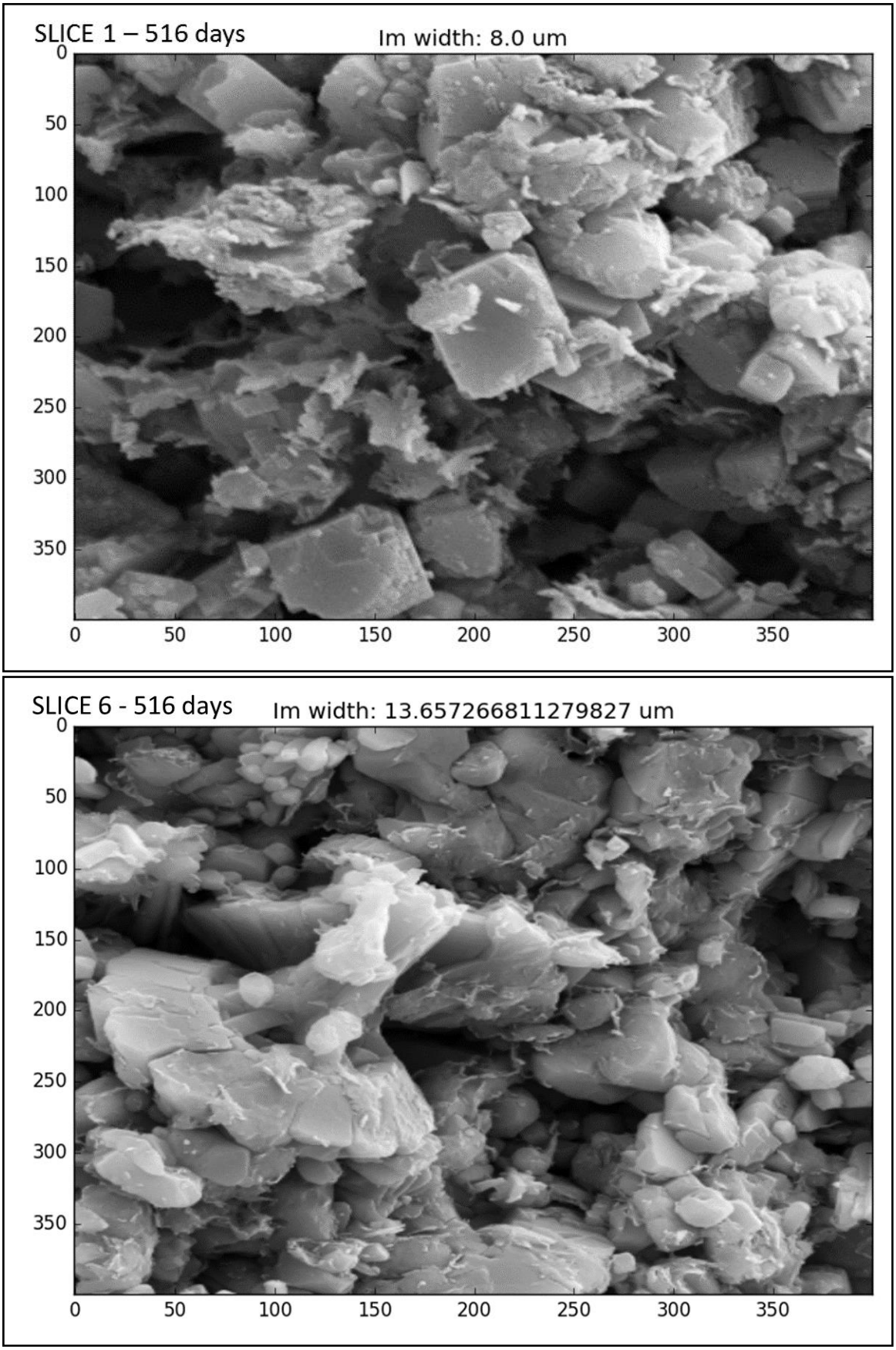

Figure 2 SEM image of Liège chalk flooded 516 days using $MgCl_2$ brine at 130°C. Slice 1 and slice 6, after 516 days $MgCl_2$ flow, can be seen.

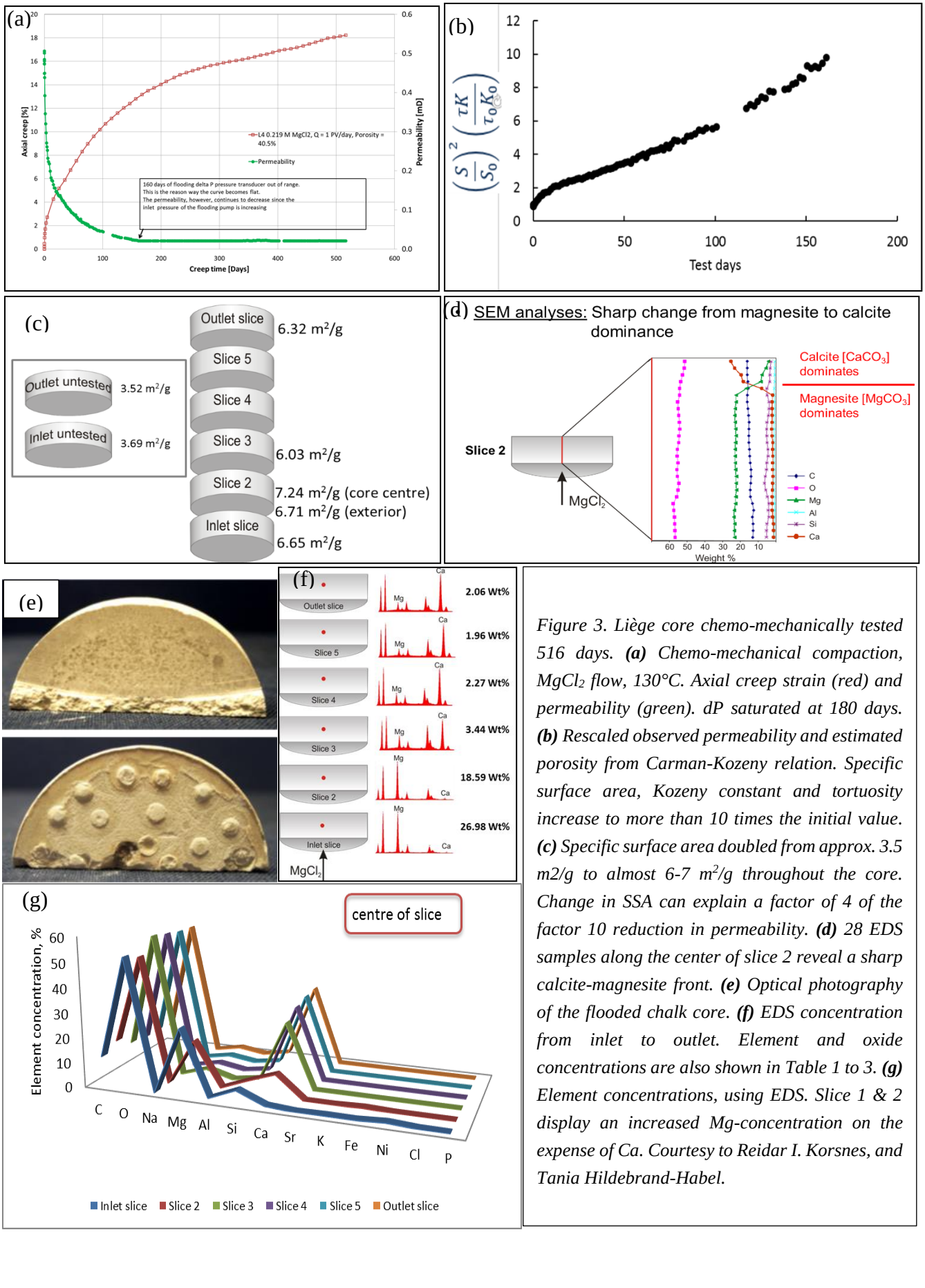

Figure 3. Liège core chemo-mechanically tested 516 days. ***(a)*** *Chemo-mechanical compaction, $MgCl_2$ flow, 130°C. Axial creep strain (red) and permeability (green). dP saturated at 180 days.* ***(b)*** *Rescaled observed permeability and estimated porosity from Carman-Kozeny relation. Specific surface area, Kozeny constant and tortuosity increase to more than 10 times the initial value.* ***(c)*** *Specific surface area doubled from approx. 3.5 m2/g to almost 6-7 m^2/g throughout the core. Change in SSA can explain a factor of 4 of the factor 10 reduction in permeability.* ***(d)*** *28 EDS samples along the center of slice 2 reveal a sharp calcite-magnesite front.* ***(e)*** *Optical photography of the flooded chalk core.* ***(f)*** *EDS concentration from inlet to outlet. Element and oxide concentrations are also shown in Table 1 to 3.* ***(g)*** *Element concentrations, using EDS. Slice 1 & 2 display an increased Mg-concentration on the expense of Ca. Courtesy to Reidar I. Korsnes, and Tania Hildebrand-Habel.*

Table 1 Weight concentration of oxides from 8 samples of the inlet-side and 7 samples from the outlet slice of unflooded Liegè chalk. Average and upper and lower bounds are reported. Upper and lower bound are shown and their values depend upon scanning domain size and position.

	Outlet side (8 samples)			Inlet side (7 samples)		
	Lower bound Wt.%	Upper bound Wt.%	Average Wt.%	Lower bound Wt.%	Upper bound Wt.%	Average wt. %
SiO_2	3.4	5.2	4.3	3.69	5.53	4.79
MgO	0.4	0.4	0.4	0.32	0.48	0.38
CaO	48.1	61.5	53.1	49.9	54.5	52.54
Al_2O_3	0.6	1.1	0.9	0.8	1.41	1.06

Table 2 Weight concentration of different oxides and elements from 27 SEM-EDS measurement of slice 1 (center, half way and along exterior). Upper and lower bound are shown and its value depends upon scanning domain size and position.

Elements and oxides	Average wt.%	Lower bound Wt.%	Upper bound wt.%
Ca	4.96	0.0	26.7
Mg	21.49	5.7	28.5
Al	0.91	0.4	4.4
Si	4.94	1.7	19.0
SiO_2	11.53	0.0	62.0
MgO	41.77	11.1	55.4
CaO	1.37	0.5	6.7
Al_2O_3	1.83	0.6	7.0

Table 3 Weight concentration of different oxides and elements from 22 EDS measurements from slice 6 (center of the core, halfway, and at the exterior of the sample). Upper and lower bound are shown and its value depends upon scanning domain size and position.

Elements and oxide weight concentration	Average wt. %	Lower bound Wt. %	Upper bound Wt. %
Ca	34.19	27.8	38.9
Mg	2.19	1.6	3.0
Al	0.40	0.3	0.6
Si	2.66	1.9	3.7
SiO_2	5.69	4.6	6.5
MgO	3.63	2.7	5.0
CaO	47.84	35.0	69.9
Al_2O_3	0.76	0.6	1.1

2 Theory

The underlying mathematical description behind the Python implementation is described in the Apendix in which Espen Jettestuen describe the implementation. The mathematics is based on a reflection of what it means to see - what does it mean to observe? The notion is that the basics of 'seeing' is related to two mechanisms: We look at colors and shapes from contrasts (gradients) in colors. For each point in the new segmented image, termed f, we chose one of the N spin-states that best match the grey-tone of the image we want to analyse g. In the generated image f we associate a cost for having a different spin-state in the neighborhood of each point. The cost of the mismatch is balanced with the cost of having a domain boundary (i.e. another grain in f) nearby. In the rest of the report we use the value S for the cost of having a surface, as such, increasing S increase the cost of having a surface, which indirectly allows larger mismatch in the grey-tone i.e. $(f - g)$ at point i. The code is 2dimensional, and as such the results are based on the assumption that the results of any 2d cross-section can represent the 3d nature of the object at study.

3 Results

The fast implementation scheme has been employed to quantify microscopic morphology of SEM images, acquired by Tania Hildebrand-Habel of a core that was flooded for 516 days by Reidar I. Korsnes. In the implementation scheme the value of S is varied. The cost parameter S is controlling the relative importance of the surface between domains relative to the grey-scale match between the grey-tone of the SEM image and one the N available values in f (i.e. grey-scale match). As such increasing S values would reduce odds of keeping the smallest grains. Domain boundaries are plotted on top of the original images in the upper panes of *Figure 4*, *Figure 5*, and *Figure 6*. The domains themselves are shown below.

Values of $S = [0.001, 0.002, 0.004, \ 0.016, 0.064, 0.256, 0.512]$ have been employed in the analysis to explore if stable specific surface area and grain size distributions could be obtained. In addition, $N = 5$ possible spin states were allowed in the presented analysis. This parameter was not changed in these runs. The images analyzed are shown in *Figure 1* and *Figure 2*. Domains and boundaries between domains are being generated in the Mumford-Shah algorithm. Each domain is meant to describe a grain in the image. For each domain, we assign an area and a perimeter length in units μm (red lines indicate the perimeter of the domains in *Figure 4*, *Figure 5*, and *Figure 6*). The impact of the value of S for the final image can be seen in *Figure 7* where $S = 0.512$ and 0.001 is seen. More small domains are seen when S is low because of the low cost of having grain boundaries.

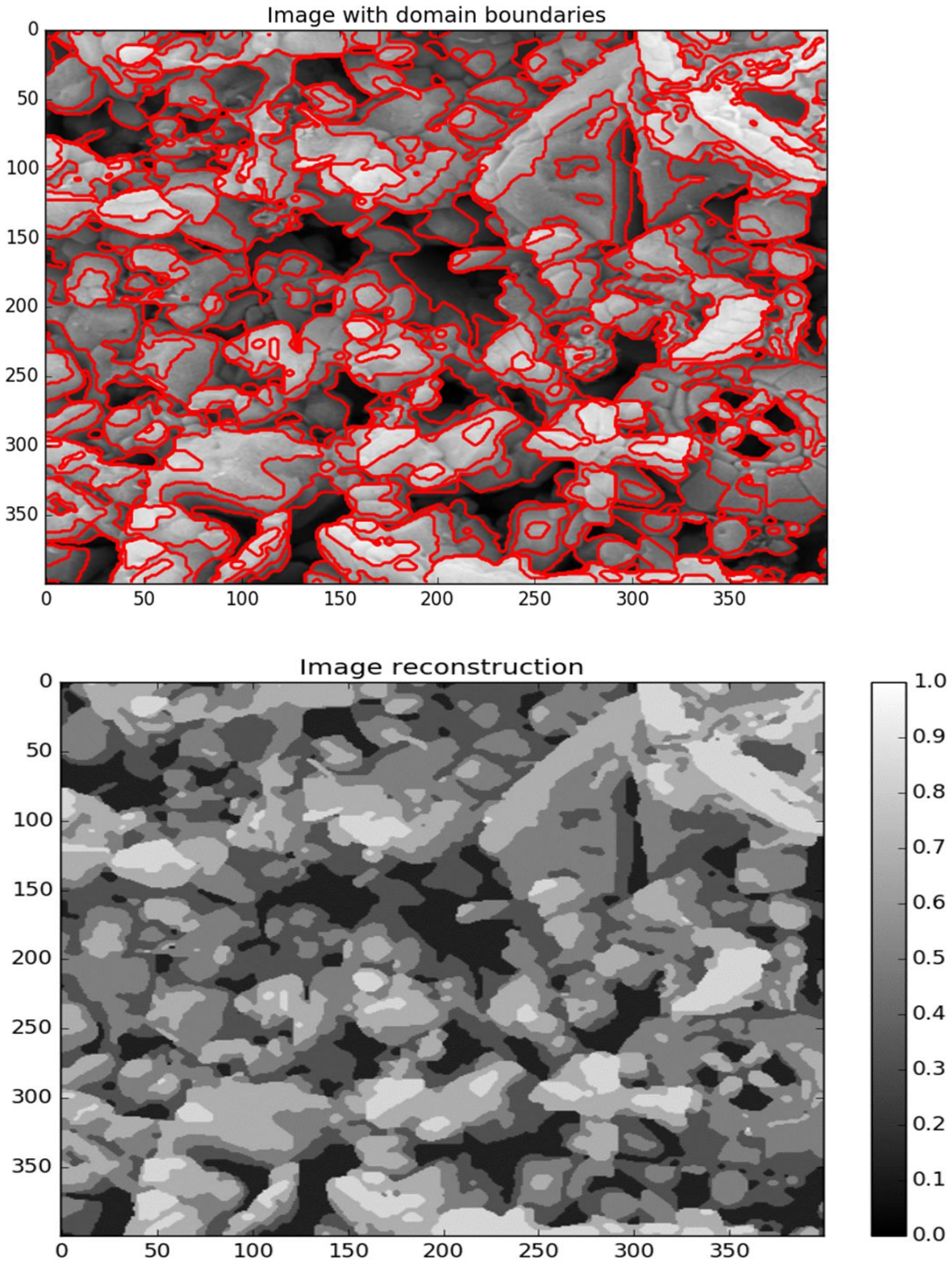

Figure 4. Unflooded chalk. Upper image display the countours of each domains shown in below. Parameters used are S=0.016 and N=5.

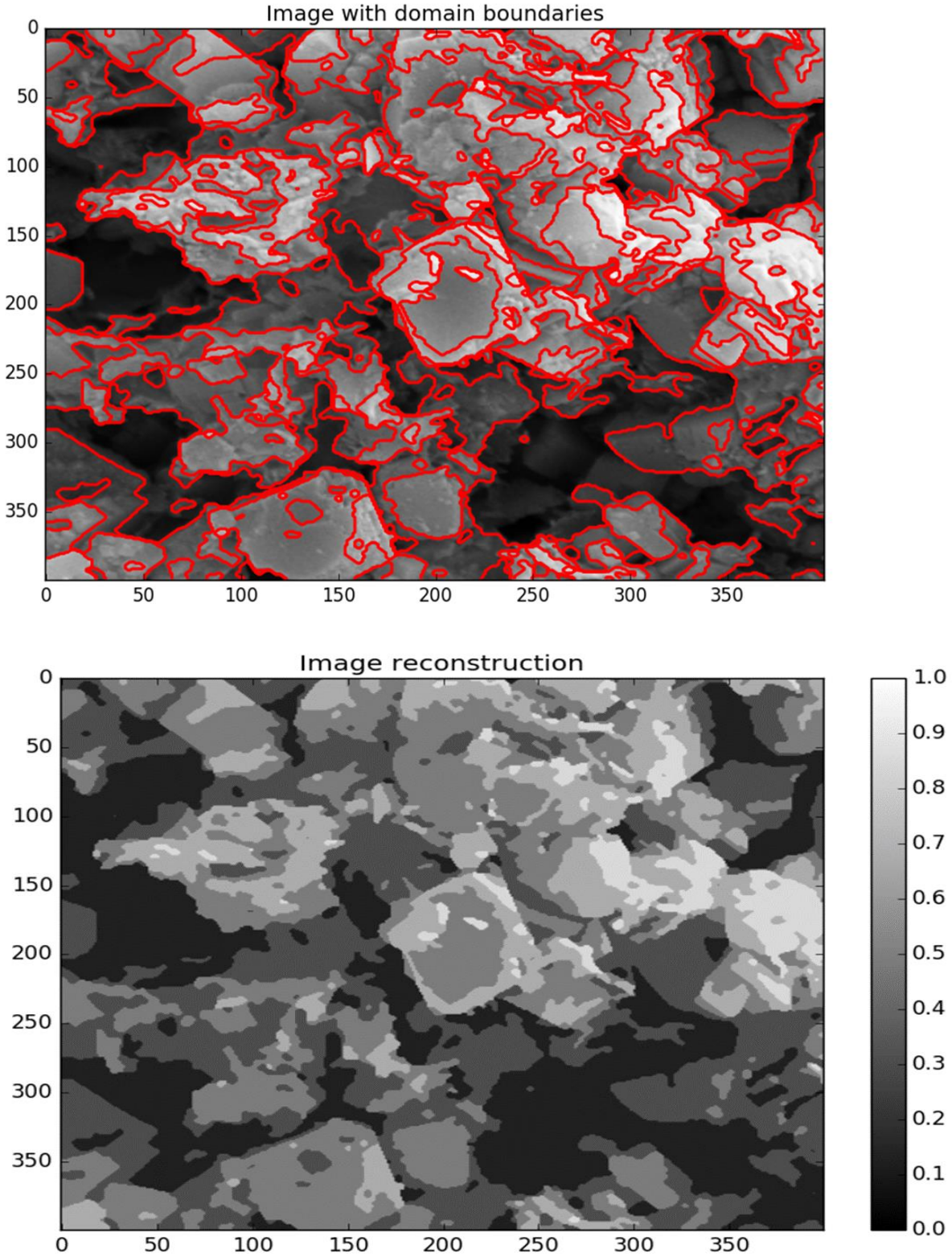

Figure 5. Slice 1 of the Liège chalk flooded by $MgCl_2$ for 516 days. Upper image display the contours of each domain as shown below. Parameters used: S=0.016 and N=5.

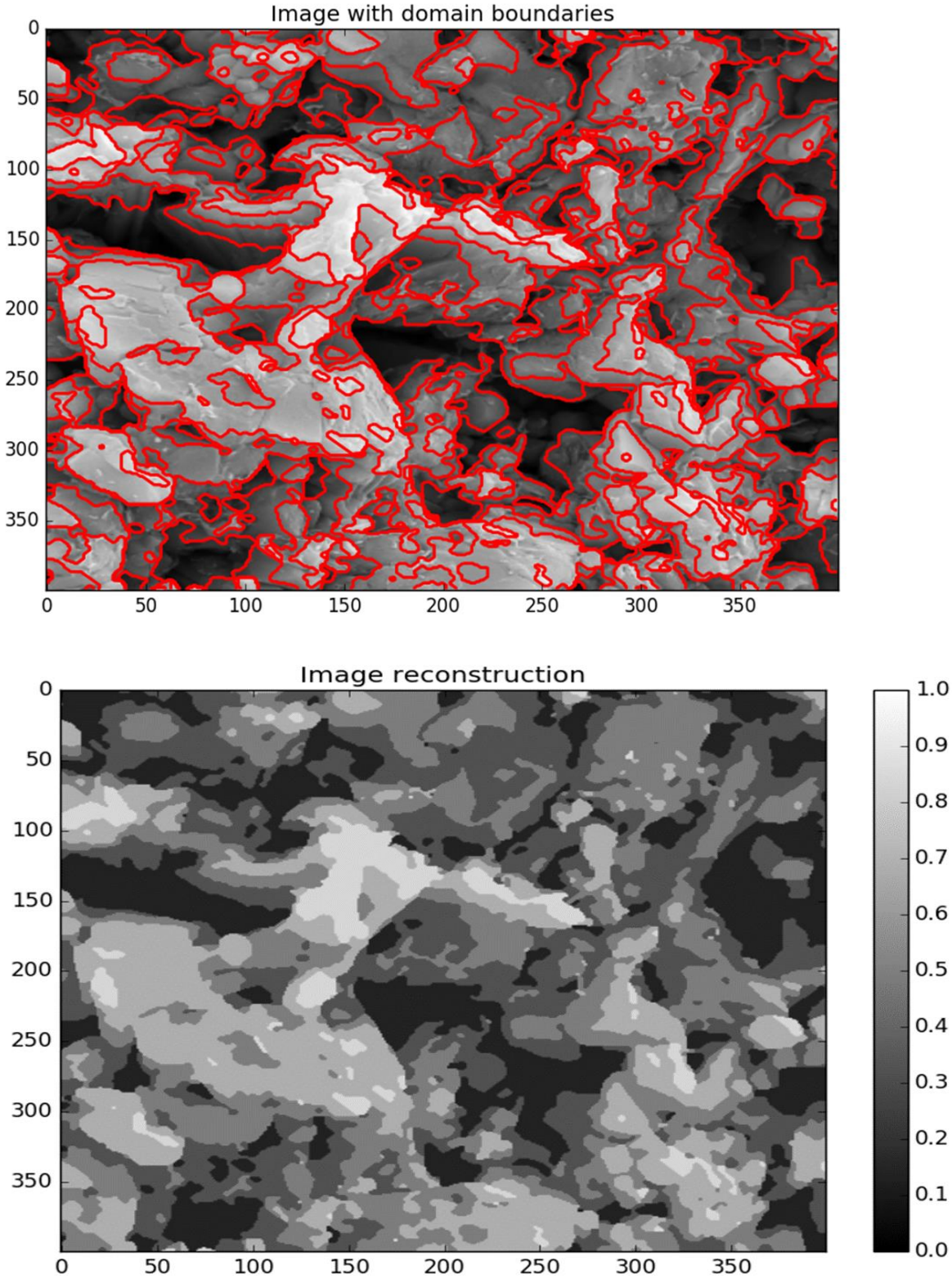

Figure 6 Slice 6 (outlet side) of Liège chalk flooded with $MgCl_2$ for 516 days. Upper image display the contours of each domain as shown below. Parameters used: S = 0.016 and N = 5.

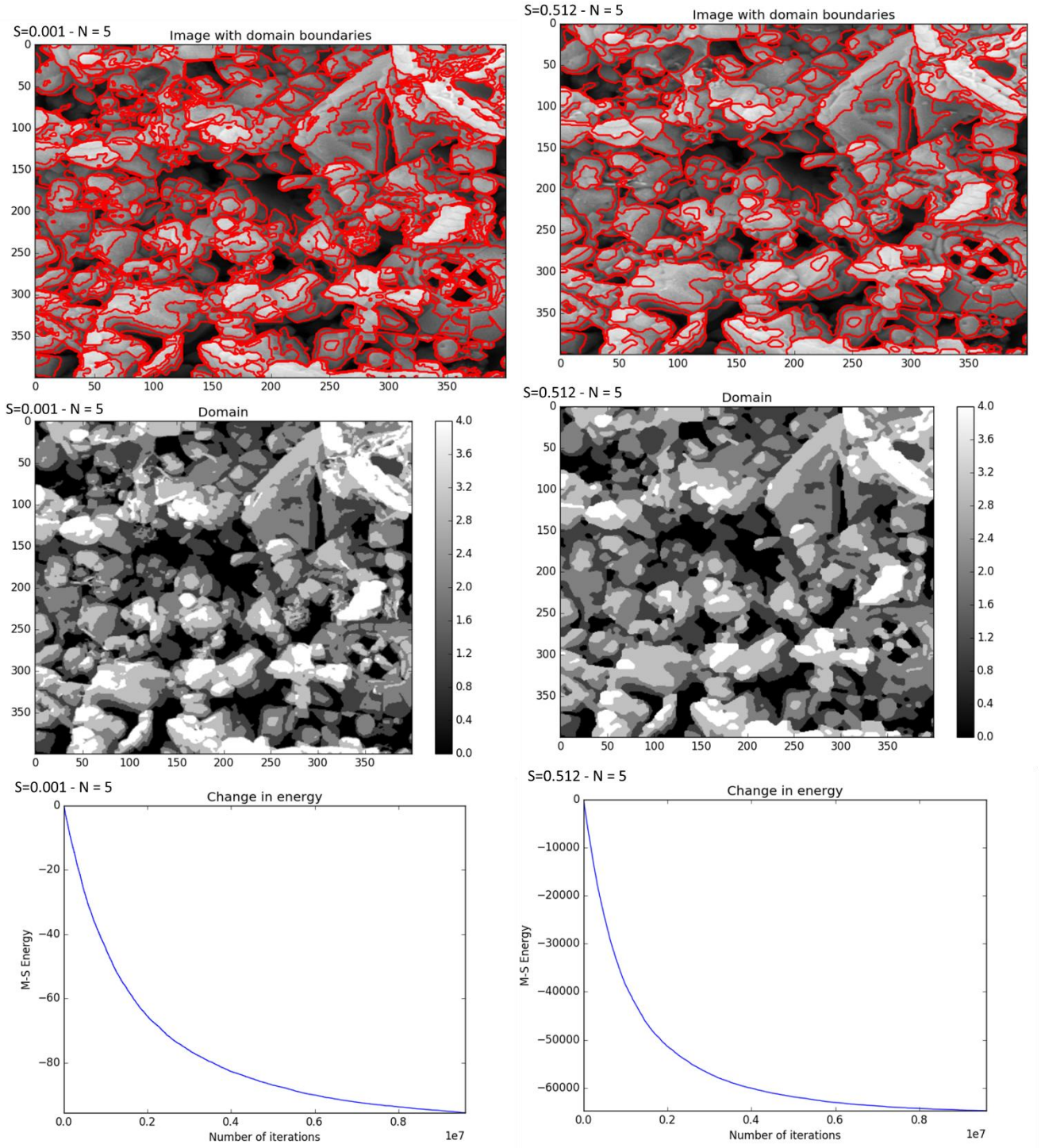

Figure 7. Unflooded Liège chalk. Left image display the grey-scale SEM image with the boundaries of the segmentation tool (red) using S=0.001 while the right pane displays S=0.512. Domain reconstruction with N=5 different spin states are shown below. Lower panes display the energy minimization after 10 million iterations. The value of S describes the relative importance of the energy cost associated with having boundaries compared to the grey-scale match of the domain.

3.1 Specific surface area measurements

Given the domains we may plot grain size distributions for each case for varying values of S, as can be seen in *Figure 9*. The code has to be compared to specific surface area measurements obtained independently using the BET-technique. The BET specific surface area is given in units [m^2/g]. Before addressing the specific surface area in detail, it is important to acknowledge that specific surface area can be defined in more than one way. Here, we defined specific surface as the ratio of the surface of all the grains divided by their total volume. In that case, it would be given in units [$\mu m^2/\mu m^3=\mu m^{-1}$]. Assuming that the cross-section is representing the 3D structure, it would be equivalent to measuring area-to-volume ratio as measuring the circumference-to-area ratio in 2D cross sections. This relies on the assumption that one can make a cross-section and it would yield a representative image of the three dimensional morphological structure. If so, we can use the boundary areas and boundary circumference that is an outcome of the developed MS-software. In our case the domain sizes and circumferences are measured in number of pixels that needs to be converted to micrometer square and length, respectively (x-axis in *Figure 9*).

Given that we now have the specific surface area in units μm^{-1} we convert to m^2/g by dividing by the grain density and convert from micron and cm^3 to meter,

$$\left[\frac{1}{\mu\mathrm{m}\cdot 10^6\mu\mathrm{m/m}}\right]\cdot\left[\frac{1}{2.7\frac{\mathrm{g}}{\mathrm{cm}^3}\cdot 10^{-6}\frac{\mathrm{cm}^3}{\mathrm{m}^3}}\right]=\left(\frac{1}{\rho_s}\right)\left[\frac{m^2}{g}\right]$$

As such, the value obtained from the circumference divided by the cross area (in micron to power -1) is simply divided by the solid density $\rho_s = 2.7\mathrm{g/cm}^3$.

The specific surface that is obtained will depend on the value of S, as the smallest and angular domains are suppressed by the surface tension. This is reflected in *Table 4* and *Figure 8*, where the specific surface area is shown for varying values of S from 0.001 to 0.512. Average specific surface areas from the shaded regions (i.e. $S > 0.016$) are shown. We find the specific surface area to be 3.82 m^2/g for the unflooded chalk, which is surprisingly close to what was obtained using the BET technique (see *Figure 3*c). We also obtain an increased specific surface area in slice 1, which also is in line with what was reported in the BET. In slice 6, however, the values seem to be reduced, which is opposite to what was reported by the BET. The same parameters are plotted in *Figure 8* where the results of the specific surface area are obtained for increasing S. It seems like stable values are obtained for $S > 0.016$, below which noise is disrupting the data.

Table 4. Specific surface from unflooded Liegè chalk, and slice 1 and slice 6 for chalks flooded for 516 days. The results are from the image analysis software given as the ratio of the average circumference divided by the average area of each domain / grain.

UNFLOODED			SLICE 1			SLICE 6		
S	µm-1	m2/g	S	µm-1	m2/g	S	µm-1	m2/g
0.001	14.37	5.30	0.004	14.31	5.30	0.001	12.70	4.71
0.002	13.07	4.82	0.016	12.31	4.56	0.002	10.87	4.03
0.004	11.34	4.18	0.064	11.83	4.38	0.004	9.56	3.54
0.016	9.82	3.62	0.256	11.90	4.41	0.016	8.14	3.02
0.016	9.72	3.59	0.001	14942.7	5534.3	0.064	7.72	2.86
0.064	9.45	3.49				0.256	7.61	2.82
0.256	8.28	3.06				0.512	7.66	2.84
0.512	9.42	3.47		Avg=	4.66		Avg=	3.63
	Avg=	3.45		Stdev=	0.37		Stdev=	0.45
	Stdev=	0.33		BET=	6.7		BET=	6.3
	BET=	3.6	Change SSA		1.35			1.05

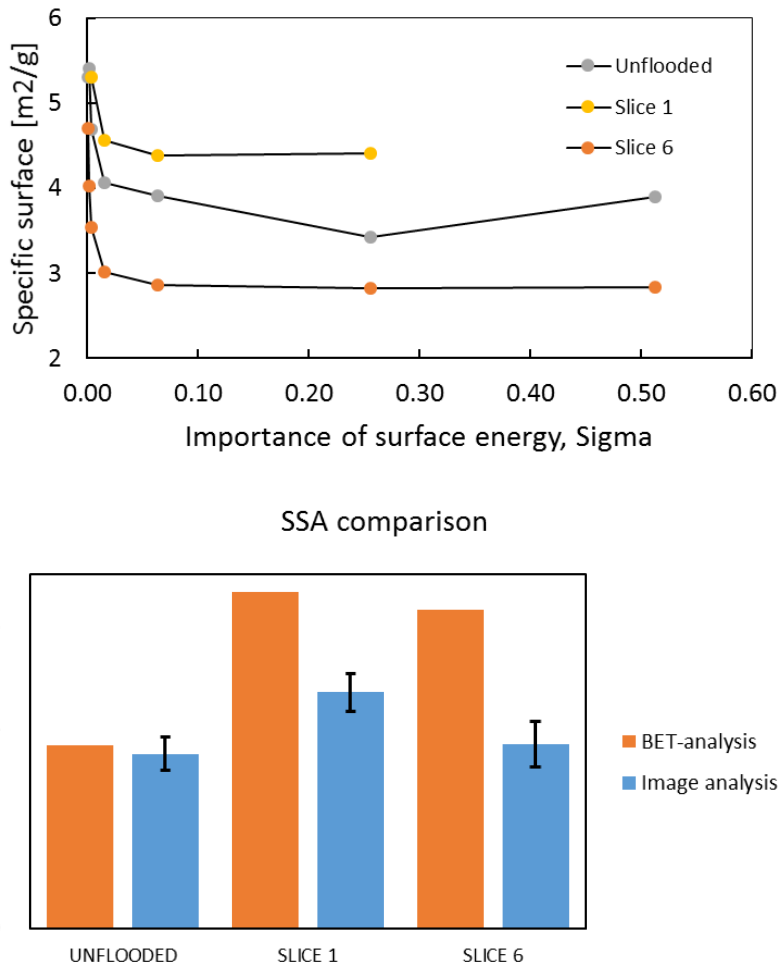

Figure 8. Specific surface as a function of the importance of surface energy in the Mumford-Shah minimization for the unflooded Liegè chalk, and slice 1 and 6 of the flooded chalk.

3.2 Grain size distribution

Given our capability to store all the areas and perimeter lengths for all domains we plot the grain size probability distributions by employing the Histogram function in Excel. In *Figure 9* these can be seen. In *Figure 9*a,b and c, the distribution of sizes can be seen for increasing values of the *S*. As can be seen, when *S* exceed approx. 0.016, the distributions collapse. The high number of domains at small values of *S* arise from the low cost of keeping several domain surfaces. In *Figure 9*d, the size probability distribution is compared for the three cores. As can be seen, slice 1 is significantly different from slice 6 and the unflooded core by the increased number of small domains (grains) and the low number of larger domains. Box sizes increase linearly with size, with the smallest domain sizes being 0.002 μm^2 (corresponding to 2 by 2 pixels) and largest 8 μm^2. Having increased probability of smaller domains lead to smaller pore throats and increased irregularities on average. Effects, which would increase the hydraulic resistance for the fluids when passing through the matrix. With this technique, we are in a better position to quantify the microscopic morphological changes.

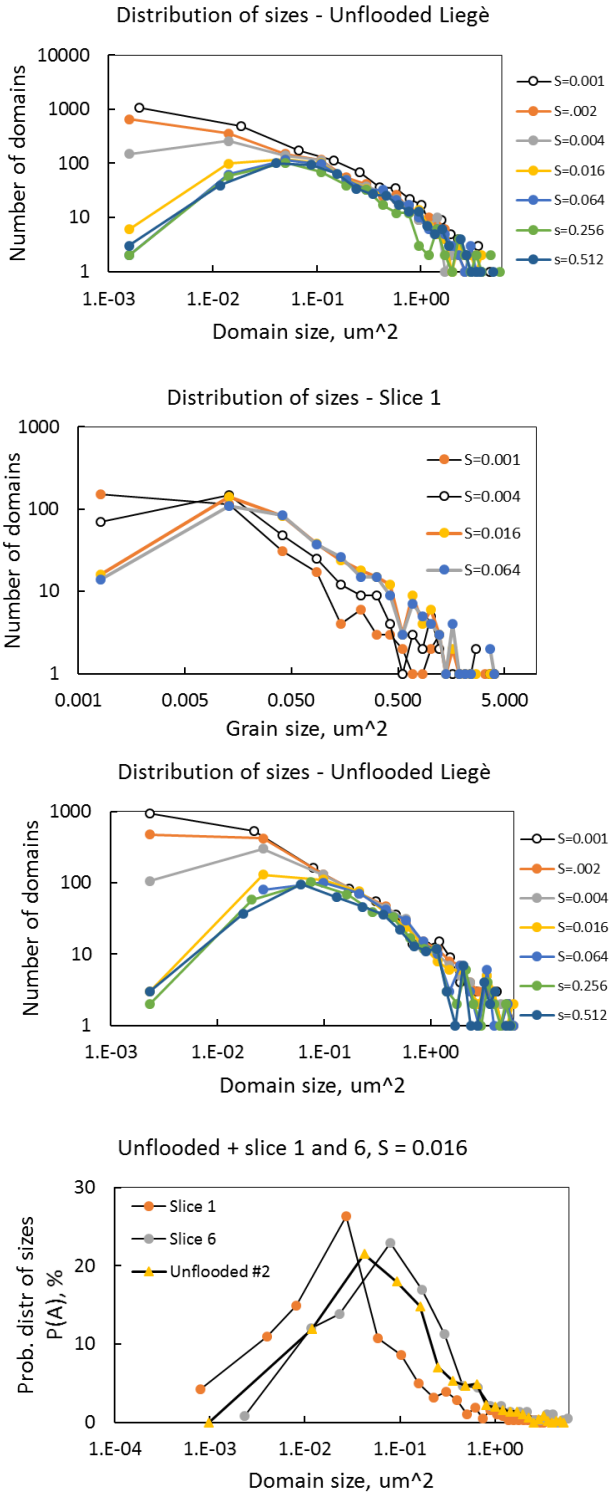

Figure 9. Distribution of domain sizes as function of the importance of surface tension term in the Mumford-Shah functional. As can be seen, for values of S=0.016 and higher, the size distributions collapse onto each other. Lower figure displays the probability distribution of sizes for each slice. As can be seen, slice 1 differs significantly from the unflooded and slice 6 by the high number of small grains that cannot be found in the unflooded and slice 6.

4 Discussion of the tools developed and results obtained

We have described a fast and simple implementation of a generalization of the binary Mumford-Shah model for image segmentation and discussed possible extensions. The standard methods to solve this problem are the level set methods. As these methods rely on advecting signed distance functions, there will be some stability issues related to the implementation. Using spin-systems we do not have these stability issues as the spins only take a fixed number of possible values. On the other hand, there are other drawbacks: 1) As we only flip one spin at a time we will need to use many iteration to get from one given configuration to another (with a maximum limit of the number of pixels in the images), which can slow down the convergence. 2) For systems with more than two spin states there exist local energy minima that have a very high multiplicity, hence the system could easily be stuck in such a state. Some of these issues could possibly be alleviated by a cunning choice of the initial configuration, but this has not been part of this project.

The method is not perfect and further extensions could aid to improve the technique. However, the software paves the way for further research into how rock-fluid interactions and mechanical compaction together affects permeability. With the objective and quantitative tool developed here we are in a position to test hypotheses that we have not been able to test before.

5 Conclusions

We have shown that porosity, and specific surface area are alone not enough to describe the permeability loss. As such, being able to better quantify the microscopic morphology is paramount to extend our understanding of chemo-mechanical compaction processes where mechanical deformation is coupled to chemical reactions. We have developed a tool that paves the way for further research in this field.

The grain size distribution and specific surface area have been quantified on SEM images of chips, broken off from the unflooded and flooded cores. Significant changes can be seen by visual inspection of the images obtained. These changes are being quantified by the use of an algorithm developed in Python, by minimization of the Mumford-Shah functional that accounts for both image gradients / edges and grey-scale matching. The relative importance of grey-scale and image gradients are tuned by the parameter S in the software. The number of spin-states is a parameter in the model. In the model runs we choose the value of 5, since this would enable us to separate neighboring grains sufficiently well. A striking match with the BET specific surface area measurements are observed.

6 Future work

The following tasks should be performed:

- Extend the analysis to include several images from the same core & slice to check for variability between different SEM images.
- Make sure that the scaling of surface tension S with respect to pixel size, i.e. number of pixels per μm, is handled correctly.
- Validate the code to check the match with respect to 2D cross sections of well-defined 3D models, as can be found in Pore Network Comparison Forum (see reference for webpages).
- Develop a three dimensional segmentation analysis to match three dimensional data, as can be found in e.g [PoreNetworkComparisonForumREF].

7 References

Brox, T., & Cremers, D. (2009). On local region models and a statistical interpretation of the piecewise smooth Mumford-Shah functional. Int. J. Comput. Vis., Vol. 84, doi: 10.1007/s11263 -008-0153-5, 184-193.

Chan, T. and L. Vese. An Active Contour Model without Edges. *Scale-Space'99*, LNCS 1682:141–151, 1999.

S. Geman and D. Geman. Stochastic relaxation, Gibbs distribution, and the Bayesian restoration of images. *PAMI*, 6:721–741, 1984.

Hildebrand-Habel, Tania et al. Presentation: *Scanning Electron Microscopy – Rock-Fluid interactions as revealed by SEM-EDS*. JCR7 Technical meeting at IRIS 16th of January 2012 at IRIS, Stavanger, Norway.

Nermoen, A., R. I. Korsnes, A. Hiorth, M. V. Madland, Porosity and permeability development in compacting chalks during flooding of non-equilibrium brines: Insights from long-term experiments. Journal of Geophysical Research – Solid Earth, 120, doi:10.1002/2014JB011631, 2015.

Mumford, D. and J. Shah. Optimal approximations by piecewise smooth functions and associated variational problems. *Commun. Pure Appl. Math.*, 42(5):577–685, 1989.

Strekalovskiy, E., & Cremers, D. (n.d.). Real-Time minimization of the Piercewise Smooth Mumford-shah Functional. Pdf retrieved from the web the 22/9-2016. https://vision.in.turn.de

Vese, L. and T. Chan. A multiphase level-set framework for image segmentation using the Mumford and Shah model. *Int. J. Comp. Vis.*, 50(3)(3):271–279, 2002.

Madland, M. V. et al, Water weakening of chalk at realistic reservoir conditions. Project financed by industry partners together support from the Petromaks KMB project by the Research Council of Norway (NFR). A joint study by University of Stavanger, IRIS AS,

GEO (Denmark), and Cornell University (USA). IRIS project number: P700165 and P7001066

Web page to Pore Network Comparison forum: http://people.physics.anu.edu.au/~aps110/network_comparison/

Weinmann, A., Demaret, L., & Storath, M. (2014). Mumford-Shah and Potts Regularization for Manifold-Valued Data with Applications to DTI and Q-Ball Imaging. Munchen, Germany and Lusanne, Switzerland: http://arxiv.org/pdf/1410.1699.pdf.

Zimmermann U., M. V. Madland, A. Nermoen, T. Hildebrand-Habel, S. A. R. Bertolino, A. Hiorth, R. I. Korsnes, J.-N. Audinot, P. Grysan, Evaluation of compositional changes during flooding of reactive fluids using scaning electron microscopy, nano-secondary ion mass spectrometry, x-ray diffraction, and whole-rock geochemistry, AAPG Bulletin, V. 99, No. 5, pp. 791-805, 2015

A spin model implementation of the Mumford-Shah functional

Espen Jettestuen

1 Introduction

This is a description of a fast implementation of a simplified Mumford-Shah functional for image segmentation [1, 3].

The Mumford-Shah functional is defined as

$$E[f,\Gamma] = \mu^2 \int\int_R (f-g)^2\, dx\, dy + \int\int_{R/\Gamma} ||\nabla f||^2 dx\, dy + \nu|\Gamma|, \qquad (1)$$

where g is the original gray scale image, f is the function we want to calculate, μ and ν are parameters, and Γ represents the surface between domains.

Here we will concentrate on the implementation in the limit when $\mu^2 \to 0$. Hence, it is the $||\nabla f||^2$-term that dominates the bulk energy. In this limit, $||\nabla f||$ will be zero, so that f becomes a piece-wise constant function for each region. By choosing f to be the mean of g in a given region, we will automatically minimize the bulk part of the energy. We can now write the simplified functional as

$$E[a_i,\Gamma] = \sum_i \mu^2 \int\int_{R_i} (a_i-g)^2\, dx\, dy + \nu|\Gamma|, \qquad (2)$$

where a_i is the mean of g in region i. We will also allow for that regions do not need to be simply connected.

2 Model

In the model, we will use $s(\vec{r})$ to denote the "spin" at site $\vec{r}$. The number of possible spin states are M. Each point $\vec{r} = (x, y)$ is given a neighborhood defined by a set of vectors $\vec{c}_\alpha$, where $\vec{v}$ is said to be part of the same neighborhood of $\vec{r}$ if $\vec{v} - \vec{r} \in \vec{c}_\alpha$. Each direction α is also given a weight w_α.

The surface length (and energy) is given by

$$|\Gamma| \propto \sum_{\vec{r}} \sum_{\alpha} w_\alpha (s(\vec{r} + \vec{c}_\alpha) \neq s(\vec{r})). \tag{3}$$

The bulk energy is given by

$$\sum_i \int \int_{R_i} (a_i - g)^2 \, dx \, dy \propto \sum_{\vec{r}} \left(g(\vec{r}) - a_{s(\vec{r})} \right)^2, \tag{4}$$

where a_i is the mean value of the g's that are part of the domain with spin $s = i$.

The system is solved by a Metropolis Monte Carlo method. First we randomly choose a trail site (x_t, y_t), then we we find a new spin for the site and calculate the energy of this configuration E_t. If E_t is less than the current energy. We accept the trail configuration if the trail configuration has a higher energy, we accept the trail configuration with a given probability dependent on the increase in energy.

We should mention that this model is a standard simplification of the Mumford-Shah approach (e.g. [1, 4]) as we say that sites with the same spin state are part of the same domain, with only one mean value, even though the domain can consist of disjoint parts.

3 Basic Implementation

A simple, but slow, implementation of the model is to use expressions (3) and (4) as they stand, to calculate the energy:

$$E[\vec{s}] = \sum_{\vec{r}} \left(g(\vec{r}) - a_{s(\vec{r})} \right)^2 + \sigma_0 \sum_{\vec{r}} \sum_{\alpha} w_\alpha (s(\vec{r} + \vec{c}_\alpha) \neq s(\vec{r})), \tag{5}$$

where a_{s_i} is given by

$$a_i = \frac{\sum_{s(\vec{r})=i} g(\vec{r})}{\sum_{s(\vec{r})=i} 1} \tag{6}$$

The steps in the program become:

1. set variables β, σ_0 and number of spin states
2. choose an initial spin configuration $\vec{s}_c$
3. calculate the current energy $E_c = E(\vec{s}_c)$
4. choose a random site $\vec{r}_t$ and a new random spin s_t

5. set $s(\vec{r}_t) = s_t$ and calculate the new energy $E_t = E(\vec{s})$
6. if $\exp(-\beta(E_t - E_c)) > \texttt{rand}(0,1)$ then set $E_c = E_t$ and $\vec{s}_c = \vec{s}_t$
7. if the energy is acceptable then stop else go to 4

This implementation is simple but scales badly with image size.

4 Fast implementation

A faster implementation consider only the energy difference between the current and the trail configuration, ΔE. We will also assume that the definition of the neighborhood is symmetric in the sense that if $\vec{c}_\alpha$ is a member of the neighborhood set, then $-\vec{c}_\alpha$ is also a member.

Surface energy: This quantity is simple to speed up, since it is a local measure. We also note that in the implementation of the surface energy in expression (3) we count each connected pair of positions twice, due to the symmetry assumption. The expression for the difference in surface energy by changing the spin at $\vec{r}_t$ is

$$\Delta E_{\text{surf}} = \sum_\alpha w_\alpha \left((s(\vec{r}_t + \vec{c}_\alpha) \neq s_t) - (s(\vec{r}_t + \vec{c}_\alpha) \neq s_c) \right), \tag{7}$$

where we have assumed that if $(0,0)$ is part of the neighborhood then its weight is zero.

Bulk energy: This is by first glance a global measure, but if we store the number of sites with a given spin, N_i and the mean value a_i we can calculate the change in the bulk energy by only using local values. Lets say that we have drawn the trail site $\vec{r}_t$ and the trail value $s_t = j$ (different form $s(\vec{r}_t) = i$). Then we have that $N_j^t = N_j + 1$ and $a_j^t = (N_j a_j + g_r)/N_j^t$ and similarly $N_i^t = N_i - 1$ and $a_i^t = (N_i a_i - g_r)/N_i^t$, where $g_r = g(\vec{r}_t)$ and we have assumed that $N_i > 1$. The change in the bulk energy is given by

$$\Delta E_{\text{bulk}} = (a_i - a_j)(g_r - 1/2(a_i^t + a_j^t)) + (a_i^t - a_j^t)(g_r - 1/2(a_i + a_j)). \tag{8}$$

If $N_i = 1$ we set $a_i^t = 0$.

5 Extensions

Non constant f: In the general setting, f can take different values at each point, not necessarily given by the mean value. One way to accomplish this is to say that given, a spin state, the energy, of that state, is given by the

f that minimize the bulk part of the functional. For a given spin state, we need to find f's that minimizes

$$\int\int_{R/\Gamma} ||\nabla f||^2 dx\, dy + \mu^2 \int\int_R (f-g)^2\, dx\, dy, \tag{9}$$

For the sake of argument, let's define the gradient-term as

$$\int\int_{R/\Gamma} ||\nabla f||^2 dx\, dy \propto \sum_r \sum_\alpha w_\alpha (s(r+c_\alpha) = s(r)) \left(f(r+c_\alpha) - f(r)\right)^2, \tag{10}$$

That is, we assume that the normal vector, $\vec{n}$, of the surface is proportional to $\vec{c}_\alpha$, so that by assuming $\partial f/\partial \vec{n} = 0$ we get that $f(r+c_\alpha) = f(r)$. Finding the energy of a given spin state in our approach will then amount to calculate the minimum of

$$E[\{f(\vec{r})\}] = \sum_r \left(\mu^2 (f(\vec{r}) - g(\vec{r}))^2 + \sum_\alpha w_\alpha \delta_{s(r+c_\alpha),s(r)} \left(f(r+c_\alpha) - f(r)\right)^2 \right), \tag{11}$$

where $s(\vec{r})$ and μ are given, and δ is the Kronecker delta.

General Mumford-Shah minimization: For the general formulation of the Mumford-Shah minimization problem, we would like to define where the boundary is positioned instead of changing node labels. This can be achieved by using a link based approach, rather than a node based approach.

We can then use the links as random variables with only two states: 'closed' or 'open', where 'closed' means that this link is part of the boundary. Below, we give a possible outline for a solver (probably similar to the model of Geman and Geman [2]).

The form of the functional for the bulk energy will be similar to equation (11), except that the $\delta_{s(r+c_\alpha),s(r)}$ will be replaced by a check if the link is 'open' or 'closed'. The explicit calculation of the minimum becomes more involved, and ammounts to solve a linear system of equations.

Since we are working with a discrete system, we can just give each $f(\vec{r})$ an index i, where i now identifies a single pixel position. Hence, the extreme of $E(f_i)$ is given by solving the system of equation given by $\partial E/\partial f_i = 0$.

As mentioned, it's more convenient to use the link based summation for the gradient term, which we can write as

$$\sum_k w_{\alpha_k} \gamma_k \left(f_{a_k} - f_{b_k}\right)^2, \tag{12}$$

where γ_k is zero if a link crosses a boundary and one if it is not, and f_{a_k} and f_{b_k} are the f-values at the end node of the link. We need also remember that in equation (11) we count each link twice.

We can now write the total bulk energy as

$$E_b(\vec{f}) = \mu^2 \sum_j (f_j - g_j)^2 + \frac{2}{C_2} \sum_k \gamma_k w_{\alpha_k} (f_{a_k} - f_{b_k})^2 \tag{13}$$

which is a quadratic form, that is, it can be written as $\vec{f}^T \mathbf{A} \vec{f} - 2\vec{b}^T \vec{f} + c$. Here, $\mathbf{A}$ is positive definite (due to the symmetries in the neighborhood). The minimum with respect to the f's is given by the linear system of equations

$$\frac{\partial E_b}{\partial f_i} = 2\mu^2 \sum_j (f_j - g_j)\, \delta_{i,j} + \frac{4}{C_2} \sum_k \gamma_k w_{\alpha_k} \left\{ (f_{a_k} - f_{b_k})\, \delta_{i,a_k} + (f_{b_k} - f_{a_k})\, \delta_{i,b_k} \right\} = 0 \tag{14}$$

we can now set $b_i = \mu^2 g_i$ and

$$A_{i,j} = \mu^2 \delta_{i,j} + \frac{2}{C_2} \sum_k \gamma_k w_{\alpha_k} \left\{ (\delta_{i,a_k} + \delta_{i,b_k})\, \delta_{i,j} - (\delta_{i,a_k}\delta_{j,b_k} + \delta_{i,b_k}\delta_{j,a_k}) \right\} \tag{15}$$

Calculating the energy: The f's are given by

$$\vec{f} = \mathbf{A}^{-1} \vec{b}, \tag{16}$$

hence the bulk energy, E_b, is simply

$$\begin{aligned} E_b &= (\mathbf{A}^{-1}\vec{b})^T \mathbf{A} (\mathbf{A}^{-1}\vec{b}) - 2(\mathbf{A}^{-1}\vec{b})^T \vec{b} + c = \vec{b}^T \mathbf{A}^{-1} \vec{b} - 2\vec{b}^T \mathbf{A}^{-1} \vec{b} + c \\ &= c - \vec{b}^T \mathbf{A}^{-1} \vec{b} = c - \vec{b}^T \vec{f}, \end{aligned} \tag{17}$$

where we have used that the inverse of a positiv definit matrix is also a positive definite matrix.

The surface energy is given by the sum of 'closed' links multiplied by the weight of its direction. That is, a link between node $\vec{r}$ and $\vec{r} + \vec{c}_\alpha$ will be given the weight w_α. The solution strategy is similar to the simplified model discussed previously:

1. set μ, σ
2. Choose an initial link configuration.
3. Find the f that minimizes the bulk energy
4. Calculate the current energy E_c
5. Create a trail configuration by randomly choosing a link and change its value.
6. Find the f_t that minimizes the bulk energy

7. Calculate the trail energy E_t

8. if $\exp(-\beta(E_t - E_c)) > \texttt{rand}(0,1)$ then set $E_c = E_t$ and set link value to the trail link value.

9. if the energy is acceptable then stop else go to 5

If we only want to consider the model without the gradient term in the energy we need to find the connected domains. These are given by nodes connected by 'open' links. Hence we need to extend the algorithm with a domain search.

Keeping track of the domains could also be used to speedup the general code, since the only f-values that need to be updated are the ones that are part of domains that undergo changes.

References

[1] T. Chan and L. Vese. An Active Contour Model without Edges. *Scale-Space'99*, LNCS 1682:141–151, 1999.

[2] S. Geman and D. Geman. Stochastic relaxation, Gibbs distribution, and the Bayesian retoration of images. *PAMI*, 6:721–741, 1984.

[3] D. Mumford and J. Shah. Optimal approximations by piecewise smooth functions and associated variational problems. *Commun. Pure Appl. Math.*, 42(5):577–685, 1989.

[4] L. Vese and T. Chan. A multiphase level-set framework for image segmentation using the Mumford and Shah model. *Int. J. Comp. Vis.*, 50(3)(3):271–279, 2002.